Copper/functionalized-carbon nanotubes composite films with ultrahigh electrical conductivity prepared by pulse reverse electrodeposition

Dawei Li[1,2] · Jiangli Xue[1] · Tingting Zuo[1] · Zhaoshun Gao[1,2,3] · Liye Xiao[1] · Li Han[1] · Shaofu Li[3,4] · Yafeng Yang[3,4,5]

Abstract

Carbon nanotubes (CNTs) have been proved a significant role as the reinforcement material in improving the mechanical and electrical properties of metal matrix composites due to their high mechanical properties, excellent electrical and thermal conductivity as well as unique atomic structure. In addition, the dispersion of CNTs has been a key factor in fabricating of metal-based complex especially for copper (Cu) with performance improvement. In the present paper, the well dispersion of functionalized CNTs (F-CNTs) is obtained at the first time, accompanied by using pulse reverse electrodeposition (PRED) technology, leading to formation of the ultrahigh electrical conductivity composite films of Cu/F-CNTs. These composite films exhibit an ultrahigh electrical conductivity of up to 6.1×10^7 S/m (increased by 105.4% of that international annealed copper standard, IACS), but maintain a high hardness of 82.3 HV and tensile strength of 297.1 MPa. It is believed that this work opens new perspectives to develop ultrahigh electrical conductivity composite materials and would role as electric wire for reducing energy loss.

✉ Zhaoshun Gao
gaozs@mail.iee.ac.cn

1 Interdisciplinary Research Center, Institute of Electrical Engineering, Chinese Academy of Science, Beijing 100190, People's Republic of China

2 School of Electronic, Electrical and Communication Engineering, University of Chinese Academy of Sciences, Beijing 100049, People's Republic of China

3 Dalian National Laboratory for Clean Energy, Dalian Institute of Chemical Physics, Chinese Academy of Sciences, Dalian 116023, People's Republic of China

4 State Key Laboratory of Multiphase Complex Systems, Institute of Process Engineering, Chinese Academy of Sciences, Beijing 100190, People's Republic of China

5 School of Chemical Engineering, University of Chinese Academy of Sciences, Beijing 100049, People's Republic of China

1 Introduction

The development of new kinds of nanostructure composite materials with high performance as ultrahigh electrical conductivity is very important for using in aerospace and electronical industries [1]. Copper (Cu), as the high electrical conductivity and excellent plasticity material, has been attracted tremendous attention due to their wide applications in mechatronics, aircraft manufacturing, electrical automation and other fields. Many attempts have been made to improve the properties of Cu matrix by grain refinement [2, 3] or introducing the second phase [3, 4] and so on [5–9]. With the rapid development of science and technology, the emerging new materials have broadened the selection as the reinforcement of the second phase. Carbon nanotubes (CNTs), since their discovery, have received a great deal of interest own to their unique atomic structure/dimension and fascinating properties, such as excellent electrical, high thermal and mechanical properties [10–12]. The movement of electrons in CNTs is ballistic transport with no scattering transmission [13] resulting in high current-carrying capacity on account of its unique one-dimensional nano-morphology. Therefore, the CNTs are usually considered as an ideal reinforcement for improving the properties of Cu.

Recently, there are lots of methods for preparing the composite materials of Cu/CNTs, and some progress has been made for improving the properties. Yoo et al. [14] prepared Cu/CNTs composite powders through high-energy ball grinding. Subramaniam group et al. [15, 16] obtained Cu/CNTs composites by electroplating Cu on the substrate of arrays of CNTs in situ growth. Cho et al. [17] prepared the Cu-based MWCNTs by low-pressure cold spraying, and Wang et al. [11] prepared MWCNTs/Cu composites by electrochemical deposition and hot pressing. The mechanical properties of the abovementioned composite materials have all improved significantly. However, the electrical conductivity of the composites has barely improved due to the poor dispersion of CNTs in Cu matrix. So far, it is still challenging to develop appropriate methods for CNTs uniform dispersion in Cu matrix to increase the electrical conductivity.

Pulse reverse electrodeposition (PRED) as an important method to prepare the intermetallic compound nanoparticles with the controlling morphology has been comprehensively investigated in various areas, especially for electrocatalysis [18, 19] and photo-electrochemistry [20]. Yet, synthesis of metallic and non-metallic composite films by this technique has been rarely reported [21]. In the present work, the cost-effective and scalable technology PRED has been introduced by using ultrahigh dispersion of functionalized CNTs (F-CNTs) as reinforcement for fabricating the composite films of Cu/F-CNTs. Notably, owing to the F-CNTs homogenous distributing in Cu matrix, the composite films of Cu/F-CNTs show an ultrahigh electrical conductivity up to 6.1×10^7 S/m which is increased by 105.4% of that international annealed copper standard (IACS). Meanwhile, the composite films of Cu/F-CNTs hold a high hardness of 82.3 HV, an excellent tensile strength of 297.1 MPa and the similar temperature coefficient of resistance (0.3997 ppm/℃) to annealed copper (220–240 MPa, 0.0039 ppm/℃). This study offers new insights into reduce energy loss by developing ultrahigh electrical conductivity of Cu-based composite materials.

2 Experimental

2.1 Fabrication of a stable CNTs suspension

The commercial CNTs (XFNANO, NO: XFM04) powder was used as original materials for fabricating high dispersion functionalized CNTs (F-CNTs). At first, 0.16 g CNTs powder was transferred into a 500-mL round-bottom flask and then a mixture solution of 1:3 for nitric acid (40 mL) and sulfuric acid (120 mL) was added. This system uderwent reflux condensation treatment in oil bath at 50–80 ℃ for 4–8 h. Successively, the system was cooled down to room temperature and left overnight. After that,

the supernatant liquid of mixed acid was removed and the residual products were diluted with 500 mL of de-ionized (DI) water. Because the addition of water in mixed acid medium released a large amount of heat, the addition of water was added gradually under stirring and the temperature of the mixture was kept to be below 50 °C by cooling. After adding all of the 500 mL of DI water, the mixture was centrifugation further to remove the acid. The above operation was repeated several times until the solution was neutral. At last, the mixture was filtered by using a 0.2 μm Nylon Millipore filter and the products of ultrahigh dispersion solution of F-CNTs were obtained by collecting the filter liquor.

2.2 Fabrication of Cu/F-CNTs composite films

Cu/F-CNTs composite films were synthesized in an electrolytic bath containing 1 mol/L blue copperas ($CuSO_4 \cdot 5H_2O$). A small amount of dilute sulfuric acid (H_2SO_4) was added to adjust the pH at 1~2. Bath temperature was maintained between 15 and 20 ℃. The pulse reverse electrodeposition (PRED) was carried out in a two-electrode system by using a multiple commutation pulse power supply (SMD-10P), where Cu sheet (99.99%) acted as anode and the clean titanium plate (Ti) as cathode. At first, pure Cu foil of 2 μm was deposited as a seed layer for the composite films easily peeled off from the Ti substrate. Then, the electrolyte was replaced to 1 mol/L $CuSO_4 \cdot 5H_2O$ which containing with a small amount of dilute H_2SO_4 and F-CNTs (with a concentration of 0.01–0.1 mg/mL). The composite films of Cu/F-CNTs were carried out under magnetic stirring (1 rps) to keep the electrolyte even. The positive (the current direction in which copper is deposited at the titanium plate defined to be positive) and negative current density was in the range of 100–400 mA/cm^2 and 0.005–0.015 mA/cm^2, respectively. The positive and negative pulse width was in the range of 4000–5500 μs and 2000–2400 μs, respectively. Duty cycle was 20–66%, and the plating time was 1800–3600 s. After the PRED process, the composite films of Cu/F-CNTs were peeled off from the Ti substrate. They were cleaned several times with anhydrous ethanol and distilled water, and then quickly dried with a blower.

2.3 Rolling and annealing treatment of composite films

The composite films of Cu/F-CNTs were annealed at a temperature of 300 ℃ for 1 h in an argon atmosphere by using tubular furnace. Then the structure was compacted by cold rolling. At last, the composite films were annealing again in the same conditions as mentioned above.

2.4 Characterization and performance measurement

The morphology of treated CNTs was characterized using transmission electron microscopy (TEM, JEOL2100) and atomic force microscopy (AFM, Dimension icon). And the distribution of F-CNTs in the composite films was characterized by scanning electron microscopy (SEM, ZEISS SIGMA), energy dispersive spectrometry (EDS) and Raman spectroscopy (RENISHAW inVia) using a 532 nm green diode laser. The tensile properties of composite films were performed on a tension machine (UTM-4000) under a crosshead speed of 2 mm/min at room temperature. The hardness was measured by the sclerometer (HV-1000) with the load of 200 g and holding time of 15 s. The electrical conductivity of composite films was measured by voltammetry (Keithley 2636A, Keithley 2182) at room temperature; at least 3 times, tests in each specimen were performed for the mean value.

3 Results and discussion

The fabrication process of functionalized CNTs (F-CNTs) with ultrahigh dispersion is depicted in Scheme 1. The F-CNTs prepared by a series of steps including reflux condensation, centrifugation and filtration, which is reported in the previous literature [22]. At first, the as-received CNTs are acid treated in a solution of 1:3 (nitric acid):(sulfuric acid) for reflux condensation in oil bath to remove catalysis particles and peel off the CNTs. After leaving overnight, the system is diluted with de-ionized (DI) water and then centrifuged several times to remove the acid until the system in neutral (pH ~ 7). Finally, the high dispersion of F-CNTs solution as well as filter liquor is obtained by filtration for across of 0.2 μm filter membrane (see details in experimental section). It is interesting to notice that there are at least three different forms for F-CNTs by the functionalization process, such as a few layers of small size graphene nanosheets, few layers of outer graphene nanosheets attaching to the intact inner walls of the CNTs (graphene-winged CNTs) and some short size CNTs with defect [23]. It is worthwhile to emphasize that the unique configuration as mentioned above facilitates dispersion in solution well as shown in Figure S1a, Supporting Information. Even after several months, the solution still remains high dispersion without any precipitation which is shown in Figure S1b, Supporting Information.

The structure properties of F-CNTs are characterized by electron microscopy studies. The scanning electron microscopy (SEM) image of the as-received CNTs exhibit highly entangled structure in the form of agglomerates or clusters (Figure S2a, Supporting Information). In addition, the TEM images show lots of nanotubes twisted and bent to randomly intertwine together resulting in severe agglomeration being consistent with the above mentioned facts due to large specific surface area and strong interlayer van der Waals interactions (Fig. 1a) [24]. Furthermore, the high-resolution TEM image exhibits that the CNTs have outer and inner diameters of ca. 10.8 nm and 2.1 nm, respectively, with a wall thickness of ca. 4.4 nm (Fig. 1b). Very distinguished from the as-received CNTs, the F-CNTs show an ultrahigh distribution with three different individual morphologies as mentioned above (Figure S3a and Figure S3b, Supporting Information). This was further probed by atomic force microscopy (AFM). As shown in Figure S3c, the F-CNTs exhibit the individual nanosheets consisting of several layers of graphene or graphene-winged CNTs. On the other hand, some shorts size CNTs with defect connected with few layer of graphene sheets or graphene-winged CNTs (Fig. 1c). This unique structure which is relatively individual but cross-link to each other is probably the key factor for not only profiting ultrahigh dispersion but also facilitating electron transfer. The corresponding high-resolution TEM images show that a loose structure with the wall thickness reduced to ca. 3.5 nm, again confirming the successful striping of CNTs (Fig. 1d). Meanwhile, the edge-crimped and defect-rich graphene nanosheets homogeneously attach to the intact inner walls of the nanotubes, which further illustrates that the CNTs could be partially or completely peeled off by the functionalized treatment and forming the ultrahigh dispersion solution.

The chemical compositions of F-CNTs are analyzed by different spectroscopic techniques. The energy dispersive spectroscopy (EDS) of F-CNTs, as shown in Fig. 1e, reveals

Scheme 1. The schematic for fabrication of F-CNTs from CNTs
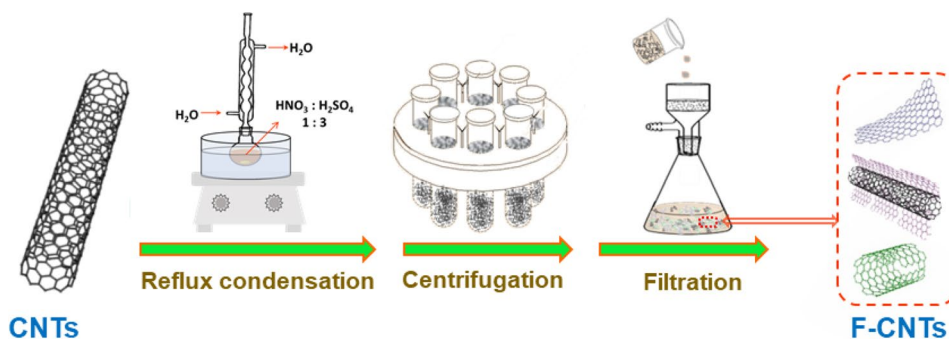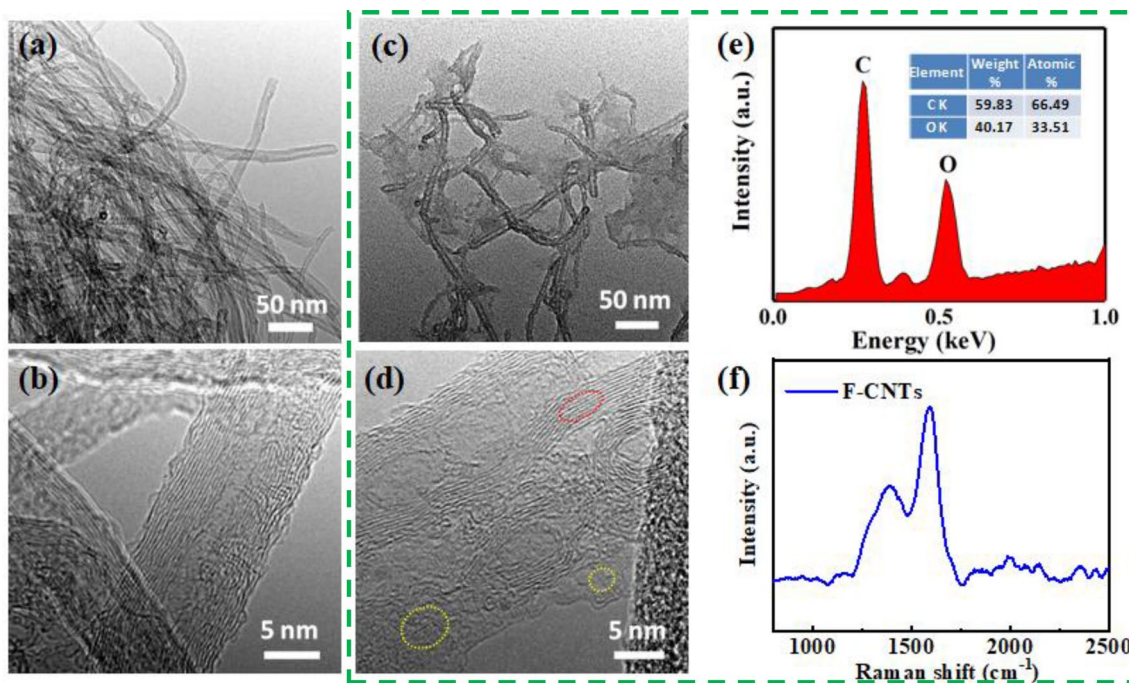
Fig. 1 **a**, **b** TEM images and the corresponding high-resolution CNTs. **c**, **d** TEM images and the corresponding high-resolution F-CNTs. **e** The corresponding EDS spectrum, and **f** Raman spectra of F-CNTs

that there are only two components of carbon and oxygen without inducing new impurities, which is corresponding with the EDS of the as-received CNTs (Figure S2b, Supporting Information). It is noteworthy that the content of oxygen component is increased obviously, implying the hydrophilic functional groups are successfully introduced resulting in the ultrahigh dispersion [25–27]. As depicted in Fig. 1f, the corresponding Raman spectrum shows that there are two strong peaks at 1350 cm^{-1} (D band) and 1580 cm^{-1} (G band), where D band represents the presence of defects indicating the partial striping of CNTs.

The PRED technology is adopted to fabricate uniform Cu/F-CNTs composite films using a titanium (Ti) sheet as the electroplating cathode and pure Cu sheet as the electroplating anode and 1 mol/L blue copperas (CuSO$_4$·5H$_2$O) with a small amount of dilute sulfuric acid (H$_2$SO$_4$) as the electrolyte (Fig. 2a). The specific details of this process are discussed in the experimental section. Furthermore, the waveform shows the current with two directions for positive and negative during the deposition (Figs. 2b, 4, Supporting Information). It is obviously seen that the positive current is not only higher than negative current, but also acting for a long time. The photo of Cu/F-CNTs film with smooth surface and uniform structure obtained by PRED technology is shown in inset of Fig. 3b, explaining the importance of pulse reverse in avoiding the formation of CNTs clusters in the matrix. To the best of our knowledge, there are no reports on Cu/F-CNTs composite films prepared by PRED technology.

To clarify the existence and uniform dispersion of F-CNTs in Cu matrix, ex situ analysis concluding SEM, EDS and Raman is conducted. The inner structure is disclosed through electrochemical-polishing and etching the surface of the composite of the Cu/F-CNTs. SEM images show the homogenous grain size of Cu matrix within the uniform distribution of F-CNTs (Fig. 2c), and the enlarged view further confirms that the F-CNTs distribute in the matrix homogenously with various morphologies aforementioned (Fig. 2d). It is clearly seen the short size CNTs and a few layers of small size graphene nanosheets, and even graphene-winged CNTs stay along in Cu. The corresponding EDS is conducted on the surface of Cu/F-CNTs composite films (Fig. 2e). From the results, a little bit of elemental carbon (5.8 wt%) exists in the composite films, again confirming the effective introduction of carbon into the copper matrix by electrochemical deposition. To further investigate the quality of the F-CNTs deposited in the composite films, Raman spectroscopy was presented as shown in Fig. 2f. It is obviously seen that there is a sharp G peak (1590 cm^{-1}) and a relative weak D (1350 cm^{-1}). The intensity ratio of the D band vs. that of G band (I_D/I_G) for F-CNTs in composite films is calculated to be 0.497, which is smaller than that of the F-CNTs (0.773) in the filtrate, indicative of low amount of defects. It means that PRED process can reduce the surface disorder and improve the electrical conductivity of F-CNTs, which is beneficial for enhancing the electrical conductivity of the Cu/F-CNTs composite films.

Fig. 2 a Schematic diagram of the experiment setup for electrodeposition. **b** Schematic representation of the pulse waveforms for co-deposition Cu and F-CNTs; the inset is photograph of co-deposition Cu/F-CNTs. **c** SEM morphology of Cu/F-CNTs, showing homogenous distribution of F-CNTs in Cu matrix. **d** The corresponding high-resolution morphology of Cu/F-CNTs, depicting the various morphologies of F-CNTs uniform dispersion in Cu matrix. **e** EDS spectra and component analysis and **f** Raman spectra of Cu/F-CNTs composite films
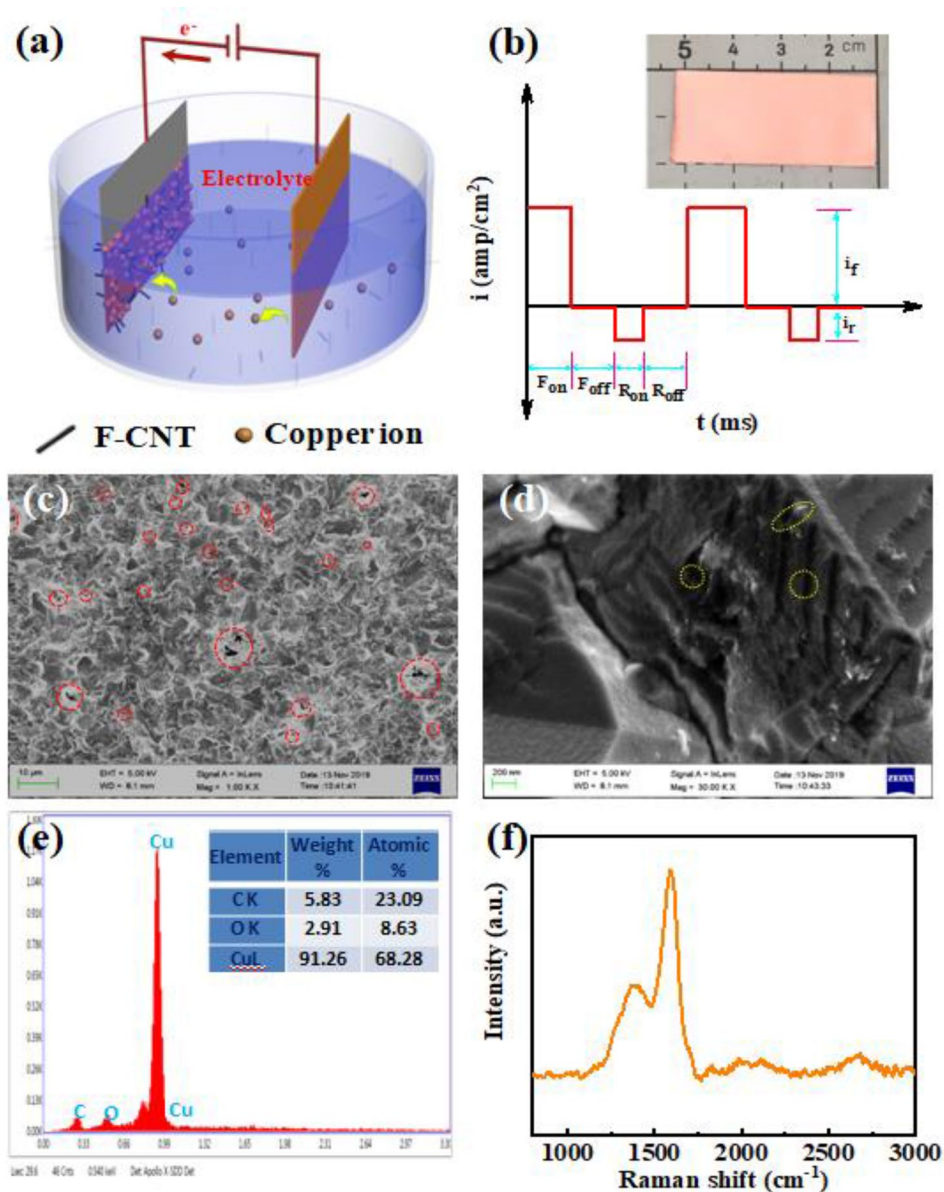
The electrical conductivity of the Cu/F-CNTs films prepared by PRED technology is evaluated by four-point probe technique, using Keithley 2636A, Keithley 2182. The experiment parameters play an important role in effecting the conductivity of composite films. So at first, the relationship between the duty cycle of cathode current and the conductivity of the composite films is studied as shown in Fig. 3a. The conductivity of the composite film decreases with the increase of duty cycle. As we all know, metal ions in the electrolyte are fully deposited in the state of cathode current conduction. Near the cathode, metal ion concentration decreases to form a diffusion layer. When the cathode current is applied continuously as well as applied in large duty cycle, hydrogen embrittlement and hydrogen branch will be formed on the surface of the coating, leading to

the degradation of the coating/depositing quality [28, 29]. Hence, on maintaining the balance between two competing growth mechanisms in PRED [30], low duty cycle results in high electrical conductivity. However, influenced by power supply equipment, the lowest duty cycle is 20%. Therefore, the highest average conductivity of up to 104% IACS is achieved at the duty cycle of 20% for the composite films.

Secondly, the cathode/anode current pulse width is adjusted, and four experiments are set up. The relationship between the conductivity of composite films and the pulse width ratio for cathode/anode current is investigated as shown in Fig. 3b. Obviously, the average electrical conductivity of the Cu/F-CNTs composite films, with whatever pulse width ratio, all can exceed 100% IACS. Especially, when the positive pulse width as 4000 μs and negative pulse
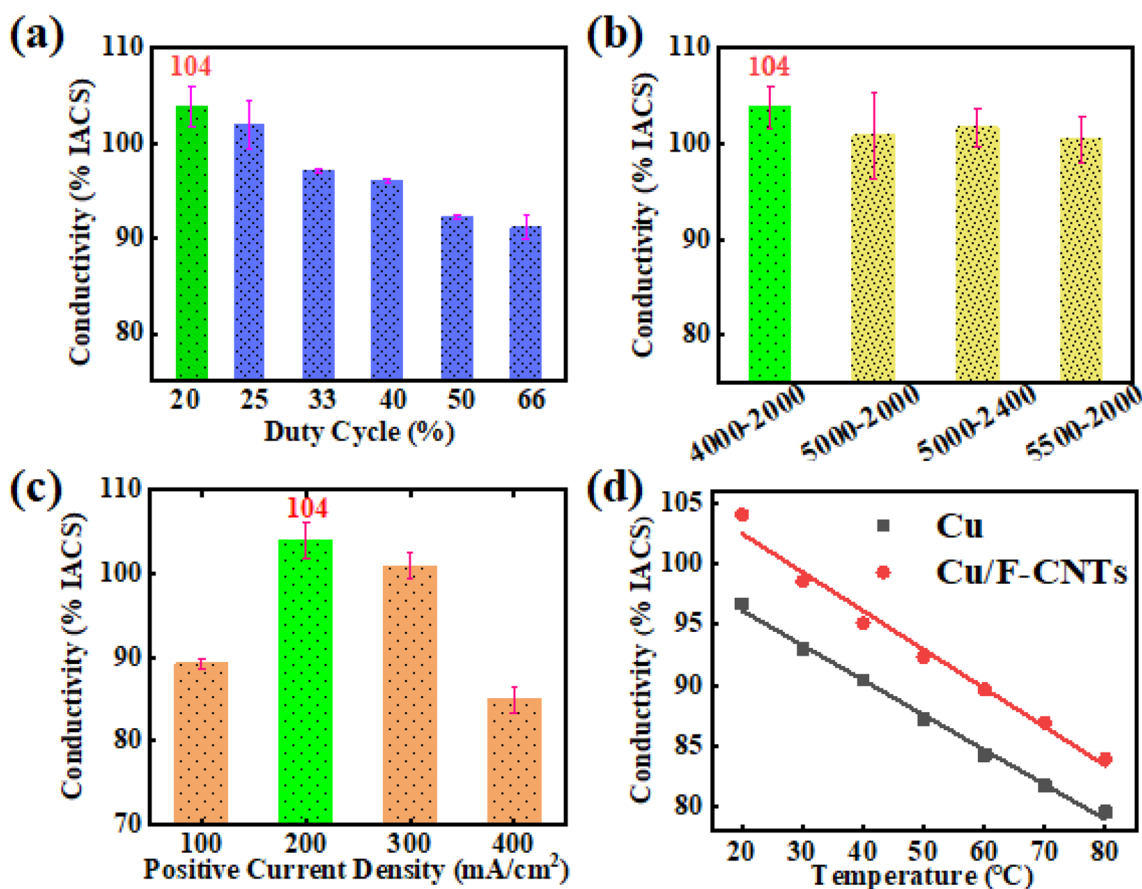
Fig. 3 The relationship between the electrical conductivity of the composite films and **a** the concentration of duty cycle, **b** pulse width (μs), **c** positive current density. **d** Conductivity temperature curve of Cu/F-CNTs composite films and the pure Cu films with the similar condition for fabricating
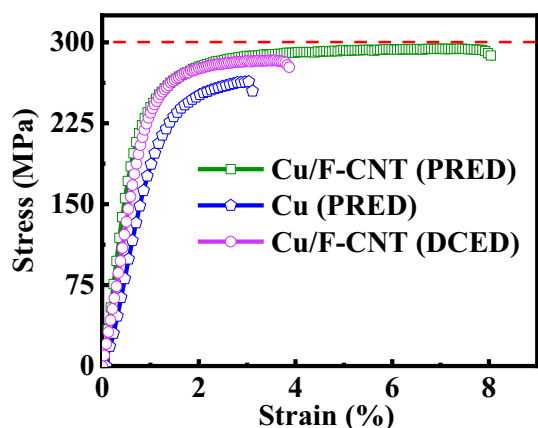
Fig. 4 The stress–strain curves of the Cu/F-CNTs films and the pure Cu films fabricated by PRED technology and Cu/F-CNTs films by DCED technology

width as 2000 μs, the conductivity reaches the highest value of 6.1×10^7 S/m (increased to 105.4% international annealed copper standard, IACS).

At last, the relationship between the electrical conductivity of Cu/F-CNTs composite films and the positive current density is discussed as shown in Fig. 3c. It is clearly seen that the electrical conductivity of the Cu/F-CNTs composite films firstly rises and then falls with the current density increased from 100 to 400 mA/cm^2. When applied with a small current density, the deposition layer consisting of large particles is loose with lots of micropores and gaps. With the current density increasing, the particles reduce resulting in dense deposits [31]. When the current density is at 200 mA/cm^2, the maximum electrical conductivity is obtained up to 6.1×10^7 S/m (increased by 105.4% of that IACS). However, if the current density is too high, severe hydrogen evolution will occur at the cathode, which will hinder the co-deposition of CNTs with the metal. Therefore, the optimal current density leads to the best deposition quality [32].

For comparison, the pure Cu films are prepared under the same condition as that of Cu/F-CNTs composite films. The electrical conductivity is calculated as 5.6×10^7 S/m, which is compared to 5.8×10^7 S/m of that IACS. Meanwhile, the direct current electrodeposition (DCED) is also

measured in this work. As expected, the Cu films and Cu/F-CNTs composite films with the rough surface (Figure S5), owning to the continuous application of current incorporation of cluster CNTs along with the Cu deposition prepared by DCED process, show lower electrical conductivity for 5.0×10^7 S/m (86.5% IACS) and 5.5×10^7 S/m (95.1% IACS), respectively. The lower results are contributed from the following elements. Firstly, it is notable that DCED is equivalent to PRED with a cathode current duty cycle of 100% and no anode current. As mentioned above, the electrical conductivity decreased with the duty cycle of cathode current increasedSecondly, by using the DCED method will lead to the loose structure with large particles for composite films, due to without reining by the anode current. Furthermore, compared with DCED, the composite films obtained by PRED are denser and have higher content of F-CNTs [29]. Therefore, PRED is advantageous over DCED for preparing pure or composite films.

The curves of conductivity with temperature of Cu/F-CNTs composite films and pure Cu films are shown in Fig. 3d. The electrical conductivity of Cu/F-CNTs films decreases as the temperature increases, which is very similar to that of the pure Cu films. According the equation below to calculation, the temperature coefficient of resistance (0.3997 ppm/℃) is kept close to that of pure copper (0.39 ppm/℃).

$$\alpha = \frac{R_2 - R_1}{R_1 \times (T_2 - T_1)}$$

The above results show that the uniform distribution of F-CNTs in the Cu matrix improves the electrical conductivity but maintains a constant temperature coefficient of resistance.

The stress–strain curves of the Cu/F-CNTs composite films and the pure Cu films fabricated by PRED technology and Cu/F-CNTs composite films by DCED technology are shown in Fig. 4. The tensile strength of Cu/F-CNTs composite films fabricated by PRED technology is observed to be 297.1 MPa. Though this value is smaller than that of MWCNTs/Cu (451 MPa) [11], it is better than that Cu/F-CNTs composite films fabricated by DCED technology (285 MPa). It is also much better than that of pure film (250 MPa) [33] and better than that of pure Cu films (261 MPa) fabricated by the similar condition due to the intrinsic high strength of CNTs. It is known that the grain dislocation by slipping is triggered under the effect of external force to release the internal stress. When the dislocation movement around the CNTs, the dislocation tangle phenomenon appears to suppress the plastic deformation process inducing new stress field and inhibiting the composite plastic deformation process, thus increasing the strength of the composite material [34].

The grain size of Cu/F-CNTs film is smaller than that of pure copper (Figure S6) because of the F-CNTs inhibiting the growth of copper grains during annealing treatment. As we all known the mechanism of fine grain strengthening, the finer of grains provide more sites for dispersion resulting in more uniformly of deformation under the same plastic deformation. There are few cracking opportunities causing by stress concentration due to few dislocations in each grain, indicating that it can bear a large deformation before fracture. Therefore, the plasticity of Cu/F-CNTs films by PRED technology composite film is higher than that of pure copper film and Cu/F-CNTs films by DCED with large particle and asymmetry structure.

Moreover, the hardness of Cu/F-CNTs composite films is evaluated by the sclerometer of up to 82.3 HV, which is slightly higher than that of pure Cu films (76.3 HV) prepared under the same conditions, but much higher than sintered Cu (48.3 HV) and CuCr/CNTs (65.3 HV) [35]. This significant improvement of hardness can be attributed to the largely reduced grain size. At first, the ultrahigh dispersion accompany with the small size of F-CNTs play the important roles in forming more nucleation cores and in reducing the grain size of the composite films, which results in increasing the hardness. On the other hand, the cold rolling is beneficial for enhancing the mechanical property as well as the reduced grain size. Therefore, it is clearly seen that the electrical conductivity and mechanical properties are all improved compared to pure Cu films after adding F-CNTs into the matrix of Cu.

4 Conclusion

In summary, Cu/F-CNTs composite films were prepared by PRED technology with ultrahigh dispersion of F-CNTs into the electrolyte exhibiting superior electrical conductivity and mechanical properties. Firstly, a stable and homogenous F-CNTs suspension with at least three kinds of morphology was fabricated by peeling or cutting off the CNTs and adding the oxygen-containing functional groups on the surface of CNTs, solving the CNTs agglomeration problem. Furthermore, by optimizing the parameters of PRED process, the Cu/F-CNTs composite film with uniform distribution of F-CNTs in copper matrix was achieved. The bonding between Cu and F-CNTs provides new pathways for electron transport and increases effective load transfer, contributing to high electrical conductivity and excellent mechanical property of Cu/F-CNTs composite films. Therefore, the ultrahigh electrical conductivity of the Cu/F-CNTs composite films is obviously up to 6.1×10^7 S/m (increased by 105.4% of that IACS). In addition, the superior mechanical properties are also obtained as the tensile strength reaches 297.1 MPa and the hardness reaches up to 82.3 HV. The

resulting composite films may reduce the energy loss for using as wires of electrical transmission.

5 Supporting information

Supporting information is available from the Journal of Materials Science or from the author.

Compliance with ethical standards

Conflict of interest The authors declare no conflict of interest.

References

1. M.E. Mendoza, I.G. Solórzano, E.A. Brocchi, Mater. Sci. Eng. A **544**, 21–26 (2012)
2. C.L.P. Pavithra, B.V. Sarada, K.V. Rajulapati, M. Ramakrishna, R.C. Gundakaram, T.N. Rao, G. Sundararajan, Cryst. Growth Des. **15**, 4448–4458 (2015)
3. Z. Li, H. Wang, Q. Guo, Z. Li, D.-B. Xiong, Y. Su, H. Gao, X. Li, D. Zhang, Nano Lett. **18**, 6255–6264 (2018)
4. S. Zhao, Y. Wu, Z. Sun, B. Zhou, X. Liu, ACS Appl. Nano Mater. **1**, 5382–5388 (2018)
5. Y.Q. Liu, Z.D. Chen, J.W. Mao, D.D. Han, X. Sun, Front. Chem. **7**, 461 (2019)
6. E. Della Gaspera, R. Tucker, K. Star, E.H. Lan, Y.S. Ju, B. Dunn, ACS Appl. Mater. Interfaces **5**, 10966–10974 (2013)
7. H. Zhang, P. Zong, M. Chen, H. Jin, Y. Bai, S. Li, F. Ma, H. Xu, K. Lian, ACS Nano **13**, 3054–3062 (2019)
8. P. Ruiz, M. Muñoz, J. Macanás, D.N. Muraviev, Chem. Mater. **22**, 6616–6623 (2010)
9. M. Ben-Sasson, K.R. Zodrow, Q. Genggeng, Y. Kang, E.P. Giannelis, M. Elimelech, Environ. Sci. Technol. **48**, 384–393 (2014)
10. A.M.K. Esawi, M.M. Farag, Mater. Des. **28**, 2394–2401 (2007)
11. Z. Wang, X. Cai, C. Yang, L. Zhou, J. Alloy. Compd. **735**, 905–913 (2018)
12. G. Chai, Y. Sun, J.J. Sun, Q. Chen, J. Micromech. Microeng. **18**, 035013 (2008)
13. O. Hjortstam, P. Isberg, S. Söderholm, H. Dai, Appl. Phys. A **78**, 1175–1179 (2004)
14. S.J. Yoo, S.H. Han, W.J. Kim, Carbon **61**, 487–500 (2013)
15. C. Subramaniam, Y. Yasuda, S. Takeya, S. Ata, A. Nishizawa, D. Futaba, T. Yamada, K. Hata, Nanoscale **6**, 2669–2674 (2014)
16. C. Subramaniam, T. Yamada, K. Kobashi, A. Sekiguchi, D.N. Futaba, M. Yumura, K. Hata, Nat. Commun. **4**, 2202 (2013)
17. S. Cho, K. Takagi, H. Kwon, D. Seo, K. Ogawa, K. Kikuchi, A. Kawasaki, Surf. Coat. Technol. **206**, 3488–3494 (2012)
18. H. Wu, Z. Zheng, C.Y. Toe, X. Wen, J.N. Hart, R. Amal, Y.H. Ng, J. Mater. Chem. A **8**, 5638–5646 (2020)
19. Y. Wang, A.S. Hall, ACS Energy Lett. **5**, 17–22 (2019)
20. H. Wu, Z. Zheng, Y. Tang, N.M. Huang, R. Amal, H.N. Lim, Y.H. Ng, Sustain. Mater. Technol. **18**, e00075 (2018)
21. C.L. Pavithra, B.V. Sarada, K.V. Rajulapati, T.N. Rao, G. Sundararajan, Sci. Rep. **4**, 4049 (2014)
22. Y.L. Yang, Y.D. Wang, Y. Ren, C.S. He, J.N. Deng, J. Nan, J.G. Chen, L. Zuo, Mater. Lett. **62**, 47–50 (2008)
23. M. Ye, C. Hu, L. Lv, L. Qu, J. Power Sources **305**, 106–114 (2016)
24. S. Cho, K. Kikuchi, E. Lee, M. Choi, I. Jo, S.B. Lee, S.K. Lee, A. Kawasaki, Sci. Rep. **7**, 14943 (2017)
25. F. Zhao, H. Cheng, Z. Zhang, L. Jiang, L. Qu, Adv. Mater. **27**, 4351–4357 (2015)
26. X.H. Wang, B.S. Guo, S. Ni, J.H. Yi, M. Song, Powder Metall. Mater. Sci. Eng. **23**, 1673–0224 (2018)
27. C. Wang, L. Zhao, J. Jia, D.Y. Wang, Z.R. Peng, Trans. China Electrotech. Soc. **34**(Sup 2) (2019)
28. X.H. Chen, J.X. Wang, X.Q. Li, S.L. Li, F.M. Deng, F.Q. Cheng, Surf. Technol. **31**, 36–39 (2002)
29. X.X. Qin, Beijing University of Chemical Technology (2010)
30. A.D. Mueller, L.Y.M. Tobing, D.H. Zhang, Adv. Mater. Technol. **4**, 1800364 (2019)
31. J.Z. Zhang Hanzhuo, L. Jianshe, L. Guangyu, J. Jilin Univ. (Engineering and Technology Edition) **37** (2007)
32. C.T.J. Low, R.G.A. Wills, F.C. Walsh, Surf. Coat. Technol. **201**, 371–383 (2006)
33. Z. Niu, W. Ma, J. Li, H. Dong, Y. Ren, D. Zhao, W. Zhou, S. Xie, Adv. Funct. Mater. **22**, 5209–5215 (2012)
34. D.H. Nam, Y.K. Kim, S.I. Cha, S.H. Hong, Carbon **50**, 4809–4814.
35. T. Zuo, J. Li, Z. Gao, Y. Wu, L. Zhang, B. Da, X. Zhao, L. Xiao, Mater. Today Commun. **23**, 100907 (2020)